Reaction mechanism in the $^{16}O+^{27}Al$ system: Measurements and analysis of excitation functions and angular distributions

Manoj Kumar Sharma,[1,*] Unnati,[1] Devendra P. Singh,[1] Pushpendra P. Singh,[1] B. P. Singh,[1,†] H. D. Bhardwaj,[2] and R. Prasad[1]

[1]*Department of Physics, Aligarh Muslim University, Aligarh-202002, India*

[2]*Department of Physics, DSN, College, Unnao, India*

(Received 26 January 2007; published 12 June 2007)

To study the dynamics of heavy ion fusion reactions in the lower mass region, experiments were carried out to measure the cross sections of radioactive residues produced in the interaction of the ^{16}O ion with ^{27}Al target nucleus at 19 different energies in very close intervals covering the energy range from ≈58 to 94 MeV, using the well-known recoil catcher off-line γ-ray spectroscopy technique. The simulation of experimental data was performed using statistical-model-based computer codes, viz., CASCADE, PACE2, and ALICE-91. The analysis of measured excitation functions indicates that these residues are likely to be produced by complete fusion, incomplete fusion, and direct reaction processes. Furthermore, to confirm the contribution of different reaction channels, a complementary experiment was performed that measured the angular distributions of the residues produced in the $^{16}O+^{27}Al$ system at 85 MeV beam energy. The analysis of the results of both experiments indicates that at these energies, the direct reactions compete with complete fusion and incomplete fusion reaction processes.

DOI: 10.1103/PhysRevC.75.064608 PACS number(s): 25.70.Gh

I. INTRODUCTION

During the last couple of decades, efforts have been made to understand the dynamics of nuclear interaction in light and heavy particle induced reactions. In light particle induced reactions, two apparently different mechanisms such as the compound nucleus (CN) and the direct reactions appear to be dominant. In the CN mechanism, the interaction between projectile and target nucleus takes place in such a way that the excitation energy is shared statistically among all the constituent nucleons of the composite system so that memory of its formation is lost. The time scales involved in these reactions are typically $\approx 10^{-16}$ s. The CN reactions are important at relatively low energies and remain a fruitful source of information about nuclear structure. On the other hand, in a direct reaction (DR), the projectile interacts with a single or a few nucleons of the target nucleus. The time taken by the projectile to traverse the target nucleus is very short ($\approx 10^{-22}$ s), thus the energy required for the DR process is relatively high, suggesting only a few degrees of freedom are involved.

Furthermore, at energies between those of the compound nucleus and direct reactions, the preequilibrium (PE) emission of nucleons has been observed, reflecting the dynamics of an excited composite system formation leading to the equilibrated CN [1,2]. In PE emission, the particle emission is assumed to take place after the first projectile target interaction but prior to the establishment of the equilibrated compound nucleus. Some of the important features of PE emission are (1) slowly descending tails of excitation function, (2) forward peaked angular distribution of emitted particles, and (3) relatively large number of high energy particles than predicated by the CN mechanism.

To explain the mechanism of such reactions, several models have been proposed. At present, model-based computer codes are available that include preequilibrium emission to explain the complete features of the experimental data. It is now possible to theoretically describe the sequence of processes, which has led to the comprehensive description of a large set of cross section data for different projectile-nucleus interactions.

In recent years, with the availability of medium energy heavy ion (HI) accelerators, it has become possible to study the nuclei at higher excitation energies and angular momenta, where, along with complete fusion (CF) processes, such processes as incomplete fusion (ICF) or breakup fusion, deep-inelastic collision (DIC), quasielastic collision (QEC), direct reaction (DR), transfer reaction (TR), PE emission, etc., are also likely to occur [3]. Thus, in HI reactions, the cross section is shared predominantly among the following processes: those leading to complete fusion, deep-inelastic collision, and quasielastic collision.

As the energy increases, one observes, in addition to light particles, beam like particle also, evidently emitted at an early stage of the reaction known as ICF particles. This emission is referred to as breakup fusion or ICF. The interplay between fusion and breakup fusion processes takes place at beam energies as low as just above the Coulomb barrier [4–9]. This observation led to a renewed interest to the study of the dynamics of HI reactions. Furthermore, the different behaviors of HI interactions, which depend on the energy regime, entrance channel mass asymmetry, etc., are still some of the unanswered and important open questions.

There are several ways to classify HI interactions. One of them is in terms of the impact parameter [3]. At higher values of impact parameter, the DR may take place, leading to few nucleon transfer processes. However, at smaller impact parameter values, the CF, ICF, and DIC processes may be dominant. In complete fusion reactions, the incident ion is

*mks_amu@rediffmail.com
†bpsinghamu@gmail.com

completely absorbed by the target nucleus, forming an excited composite system from which particles and/or γ rays may be emitted after the formation of the equilibrated compound nucleus.

However, in the case of ICF, the projectile is assumed to break up in the vicinity of the nuclear field of the target nucleus into the fragments called projectile-like fragments (PLFs), and only one of the PLFs fuses with the target nucleus, while the remaining PLFs continue to move in the forward direction with approximately the same velocity as that of the incident ion. The ICF reactions have been reported to have the following characteristics: (1) a forward peaked angular distribution of PLFs, which are predominantly emitted at the beam velocity and are generally viewed as fast breakup of the projectile, (2) a linear momentum transfer less than that of complete fusion, resulting in a smaller range of the evaporation residues, (3) a relatively higher measured cross section than that predicted by statistical models, and (4) a higher energy of the direct α particles than that of the evaporation α particles from the equilibrated compound nucleus. Various models have been proposed to describe the dynamics of ICF reactions, but none of them is able to explain the experimental data over a large energy range and mass region as well. It may not be out of place to mention that there is no satisfactory theoretical support so far for ICF reactions that can be used to simultaneously explain complete and incomplete fusion processes.

Furthermore, DICs may also be likely at these energies, in which the mass of the resulting nuclei are close to the mass of the projectile and target nuclei. The deep-inelastic collision may be characterized by substantial dissipation of initial kinetic energy and angular momentum. The time scale at which DICs are expected to occur is less than the CN lifetime, but long enough for the exchange of a significant number of nucleons between the target and the projectile. One may get the information about the mechanism through the measurement and analysis of cross section data, recoil range, and angular distributions of the residues produced in the interaction of two heavy nuclei. The cross section data obtained for such channels have a wide range of applications. Therefore, the above study is not only an important subject in its own right, but also significant for its impact on related fields of investigation and for its rich variety of applications. In this context, a program of measurement and analysis of the cross sections of nuclear reactions induced by HI has been undertaken [10].

In the present work, the excitation functions (EFs) for radioactive residues produced in the interaction of ^{16}O ion with ^{27}Al have been measured in order to study the reaction dynamics, particularly in the low mass region. Most of the studies in which the occurrence of ICF was observed were carried out generally with heavier mass target nuclei. Though initial studies on incomplete fusion have been carried out at energies $\approx$10 MeV/nucleon using rare-earth targets [11], there are very few studies with lower mass target nuclei. One advantage of using a lighter mass system is to avoid the possibility of fission, which is one of the competing modes in HI reactions on heavier target nuclei at these energies. Furthermore, if heavier targets are used, the emission of α particles from the fused excited system is likely to be substantially reduced [12] because of the high Coulomb barrier. As a result, the emission of α particles in incomplete fusion channels may give rise to residues which may have very little contribution from complete fusion channels. Measurement and analysis of EFs [4,5] in HI reactions for heavier target nuclei have indicated that ICF is an important component of the reaction mechanism at these energies.

With the motivation to determine the contribution of incomplete fusion processes in light mass target nuclei, the measurement and analysis of the cross sections for the reaction channels $(2\alpha n)$, $(3\alpha 3p)$, $(3\alpha 3pn)$, $(4\alpha 2pn)$, and $(4\alpha 3p)$ produced in the ^{16}O+^{27}Al system have been carried out at 19 different energies at very close intervals covering the energy range from $\approx$58 to 94 MeV. There are mainly two experimental methods which are widely used to study the dynamics of HI reactions: (1) off-beam γ-ray spectrometry by the measurement and analysis of the excitation functions (EFs), recoil range distributions, and angular distributions of the residues produced in the projectile-target interaction using the activation technique and (2) in-beam γ-ray spectrometry by detecting the breakup α particles of the projectile, i.e, projectile-like fragments, in coincidence with the prompt γ rays of the populated residues using the particle-γ coincidence technique. The former is based on the measurement of the activity produced in radioactive residues using off-line γ-ray spectroscopy.

In the literature [13], the measurement of cross section data exists for the ^{16}O+^{27}Al system using the activation technique. Landenbaurer-Bellis *et al.* [13] measured the cross section for the reactions in the above system employing the activation technique in the energy range 10.5–1 MeV/nucleon, using a NaI (Tl) detector to identify γ rays of interest and an end-window gas flow proportional counter to resolve β decay. The energy spread of the data points are substantially large. It may, however, be pointed out that no theoretical interpretation of the data was made [13]. Furthermore, it has been mentioned that observed trend of the data indicates a CN mechanism. However, more recently, McKenna *et al.* [14] tried to reproduce the experimental data [13] in an experiment using a high intensity laser produced plasma beam. They also performed theoretical calculations [14] using the Monte Carlo code PACE2 [15]. They reported that residue ^{34}Cl is produced by the evaporation of two α particles and one neutron from the compound nucleus. Furthermore, the production of other radioisotopes, viz., ^{27}Mg, ^{24}Na, and ^{24}Ne, was attributed to the compound nucleus as well as to direct reactions. It is not out of place to mention here that incomplete fusion and deep-inelastic collision are also dominant mechanisms in HI reactions at these energies, and hence the contributions of these reaction channels are also required to be taken in to account.

In the present work, an attempt has been made to explain the experimentally measured cross sections using statistical-model-based computer codes, viz., CASCADE [16], PACE2 [15], and ALICE-91 [17]. To obtain complementary information about the processes involved in lighter mass symmetric systems, angular distributions of the residues produced in the ^{16}O+^{27}Al system have also been measured at 85 MeV beam energy. Experimental details are discussed in Sec. II of the paper; the analyses of the excitation functions and angular distributions are presented in Secs. III and IV, respectively. Conclusions are given at the end of the paper.

II. EXPERIMENTAL DETAILS

The experiments were performed at the Inter University Accelerator Centre (IUAC) formerly known as Nuclear Science Center (NSC), New Delhi, India, using the 15 UD Pelletron accelerator facility. The experiments for excitation functions and angular distribution measurements were carried out in the general-purpose scattering chamber (GPSC) of 1.5 m diameter dedicated for such studies, having an in-vacuum transfer facility. The time interval between the end of irradiation and the beginning of counting was minimized using in-vacuum transfer of samples from the scattering chamber to the counting system. Details of the measurements of excitations functions and annular distributions are given in the following subsections.

A. Excitation functions

The spectroscopically pure self-supporting foils of ^{27}Al (purity ≈99.999%) were rolled to obtain samples of the desired thickness. Target thickness plays a crucial role in each measurement. Therefore, measurement of target thickness must be as accurate as possible to obtain accuracy in the measured cross section data. In the present case, the thicknesses of the target as well as the catcher foils were determined using the α-transmission method. This method is based on the measurement of the energy lost by 5.485 MeV α particles obtained from a ^{241}Am source while passing through the target thickness. For thickness determination, the stopping power values were calculated using the program SRIM-2006. The measured thickness of ^{27}Al foils were ≈1.8 mg/cm^2. The Al samples and the degrader/catcher foils were cut into 1.2 × 1.2 cm^2 squares and pasted onto rectangular target holders having concentric holes of 1.0 cm diameter. In the present work, two stacks containing five alternating samples of natural Tm and Al and another two stacks containing five and four alternating samples of natural Tb and Al, respectively, were used for the EF studies. The samples of Tm and Tb served as energy degraders and catchers. In separate communications [18,19], the activations of the Tb and Tm samples were studied for the measurement of cross sections for a large number of channels. The calculations of energy loss in the stack were done using the energy range program SRIM-2006. Four stacks containing in all 19 ^{27}Al samples and an equal number of energy degraders were irradiated by the $^{16}O^{7+}$ beam at four different energies, i.e., 86, 88, 92, and 95 MeV. The irradiation of these four stacks covered the desired energy range ≈58 to 95 MeV. As the beam traverses the samples of the stack, the energy spread goes on increasing toward the last sample. As a typical example, the energy spread at ≈58 MeV is ≈2%. Keeping in mind the half-lives of interest, the irradiation of each stack was carried out for ≈8 h duration. The beam currents were ≈50 nA. The total charge collected in the Faraday cup was used to calculate the flux of the incident beam. Furthermore, to monitor the flux of the incident beam, in an auxiliary experiment, two Rutherford monitor detectors kept at ±30° with respect to the beam direction were used. The two readings of the flux agreed with each other within an uncertainty of about 5%. It may, however, be pointed out that the unreacted beam is dumped in the Faraday cup about 1 m away from the samples.

In the present work, the analysis of the $^{16}O+^{27}Al$ system is being presented which provides a data set of 19 points at very close energy intervals. The stacked foil activation technique followed by off-line γ-ray spectroscopy was employed to determine the cross sections for various reaction residues. In the stacked foil technique, the energetic beam traverses through all the samples with degrading beam energies; as such, it is possible to bombard different samples of the stack at different energies. The activities induced in the various samples were recorded by counting the Al samples as well as the degrader/catcher foils using a high-purity Ge γ-ray spectrometer coupled to a personal-computer-based multichannel analyzer setup employing the FREEDOM software [20]. The counts under photo peaks of interest were taken for the determination of cross section after proper background correction. The HPGe γ-ray spectrometer (resolution ≈2 keV for 1.33 MeV γ ray of ^{60}Co) was precalibrated for both energy and efficiency employing various standard γ sources such as ^{22}Na, ^{54}Mn, $^{57,60}Co$, ^{133}Ba, ^{137}Cs, and ^{152}Eu. To determine the geometry-dependent efficiency G_ε for γ rays of different energies, a standard source of ^{152}Eu of known strength was used. A typical plot of G_ε at 2 cm distance from the sample to the detector system is shown in Fig. 1. Relevant portions of the observed γ-ray spectrum of the irradiated ^{27}Al sample at 82 MeV ^{16}O beam are shown in Fig. 2.

The peaks in the observed γ-ray spectrum were assigned to different reaction residues on the basis of their characteristic energy of γ lines as well as measured half-lives. A typical curve used to determine the half-life of the residue ^{34m}Cl is shown in Fig. 3. A list of reactions, energies of the identified γ rays, and their branching ratios [21] are given in Table I.

The measured intensities of the characteristic γ rays were used to compute the reaction cross sections using the formula [22]

$$\sigma_r(E) = \frac{C_a \lambda \exp(\lambda t_l)}{N_o \phi P K(G_\varepsilon)[1 - \exp(-\lambda t_i)][1 - \exp(-\lambda t_a)]}, \quad (1)$$

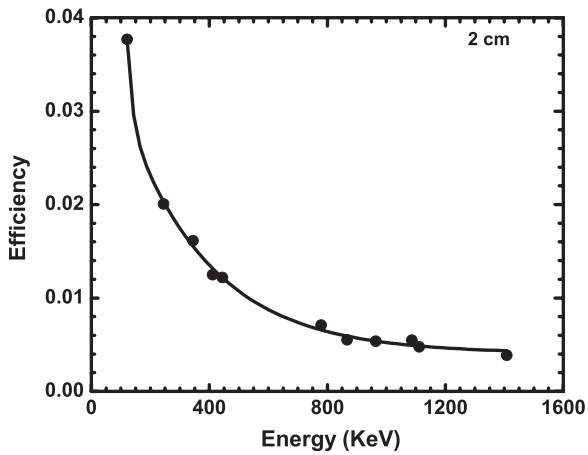

FIG. 1. Typical plot of photo peak efficiency of HPGe detector as a function of γ-ray energies of the ^{152}Eu source.

TABLE I. Reactions, measured half-lives, identified γ rays, and their branching ratios.

Sample no.	Reaction	Half-life	E_γ (keV)	Branching ratio (%)
1	^{27}Al(^{16}O, $2\alpha n$)^{34}Cl	32.2 min	146.5	40.5
2	^{27}Al(^{16}O, $3\alpha 3p$)^{28}Mg	20.9 h	400.5, 1342.3	36.0, 54
3	^{27}Al(^{16}O, $3\alpha 3pn$)^{27}Mg	9.4 min	843.7	73.0
4	^{27}Al(^{16}O, $4\alpha 2pn$)^{24}Na	14.6 h	1368	100
5	^{27}Al(^{16}O, $4\alpha 3p$)^{24}Ne	3.8 min	472.2	100

where C_a is the observed counts under the photo peak during the accumulation time t_a of the induced activity of decay constant λ, N_o the number of target nuclei irradiated for time t_i with a particle beam of flux ϕ, t_l the time lapse between the stop of irradiation and the start of counting, P the branching ratio of the characteristic γ ray, and G_ε the geometry-dependent efficiency of the detector for the γ ray of a given energy. Proper correction for the geometry-dependent efficiency was taken into account for each case. The factor $[1 - \exp(-\lambda t_i)]$, known as the saturation correction, takes care of the decay of evaporation residues during the irradiation. The corrections for the decay of the induced activity due to the delay between the stop of irradiation and the start of counting and during the data accumulation are taken into account via the factors $\exp(\lambda t_l)$ and $[1 - \exp(-\lambda t_a)]$, respectively. $K = [1 - \exp(-\mu x)/\mu x]$ is the correction for the self-absorption of the γ radiation in the sample thickness itself, where x is the thickness of the sample and μ is the energy-dependent γ-ray absorption coefficient.

The experimentally measured values of cross sections at different energies for the reactions ^{27}Al(^{16}O, $2\alpha n$)^{34}Cl, ^{27}Al(^{16}O, $3\alpha 3p$)^{28}Mg, ^{27}Al(^{16}O, $3\alpha 3pn$)^{27}Mg, ^{27}Al(^{16}O, $4\alpha 2pn$)^{24}Na, and ^{27}Al(^{16}O, $4\alpha 3p$)^{24}Ne are given in Table II.

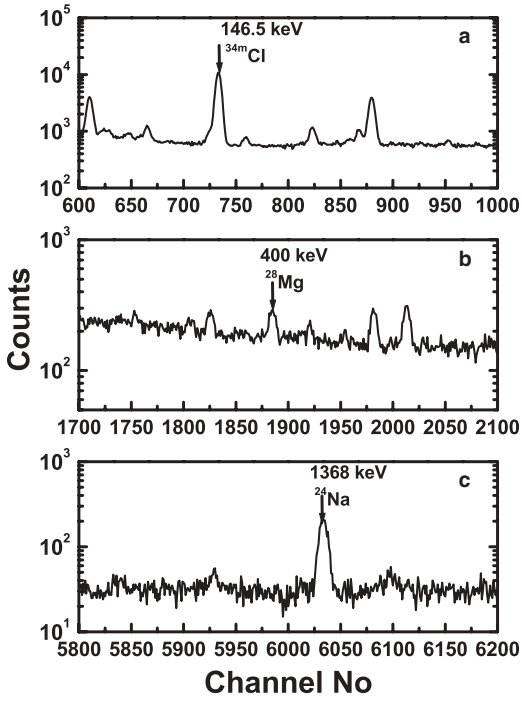

FIG. 2. Observed γ-ray spectrum of irradiated ^{27}Al sample at 82 MeV.

B. Angular distributions

A separate experiment has also been carried out to measure the angular distribution of recoiling residues produced in the ^{16}O+^{27}Al system at 85 MeV beam energy. In this experiment, an Al target supported by Tm material of thickness $\approx$0.48 mg/cm^2 followed by a stack of thick annular concentric Al catcher foils was mounted in the irradiation chamber normal to the beam direction. Concentric annular aluminum catchers of thickness $\approx$0.3 mm with diameters 0.81, 1.29, 1.95, 2.64, 3.27, 5.46, and 6.4 cm were used to trap the recoiling nuclei emitted at different angles. A typical arrangement of the target and catcher assembly used for the angular distribution measurements is shown in Fig. 4. The arrangement of annular catchers was placed 1.8 cm behind the target for collecting the residues emitted in seven different angular ranges, viz., 0°–13° (most forward cone), 13°–21°, 21°–30°, 30°–39°, 39°–45°, 45°–60°, and 60°–64°. The irradiation was carried out for about 11 h with a beam current of $\approx$7 pnA. The activities induced in each catcher were followed off line for a couple of days. Typical γ spectra indicating the region of interest for different annular Al catcher rings covering the angular range from 0°–13° to 45°–60° is shown in Fig. 5. For identification of the reaction residues, the similar procedure is adopted, as discussed in Sec. II A. Further,

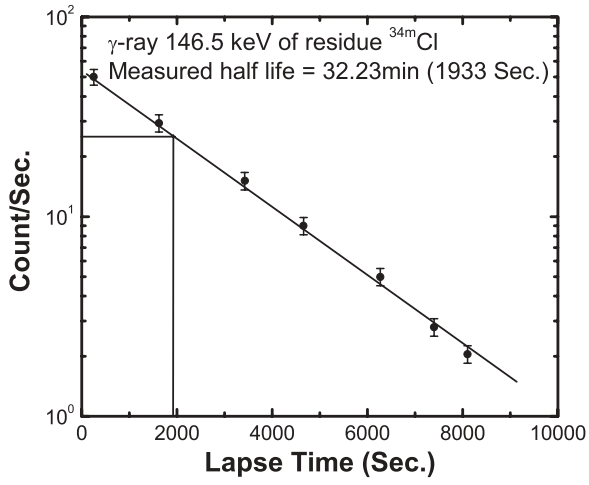

FIG. 3. Typical curve used to determine the half-live of the residue ^{34m}Cl.

TABLE II. Experimentally measured cross sections.

Lab energy (MeV)	$\sigma(^{34}Cl)$ (mb)	$\sigma(^{28}Mg)$ (mb)	$\sigma(^{27}Mg)$ (mb)	$\sigma(^{24}Ne)$ (mb)	$\sigma(^{24}Na)$ (mb)
58.0 ± 1.3	9.40 ± 1.69	–	–	–	0.46 ± 0.08
58.7 ± 1.3	14.57 ± 2.62	–	–	–	1 ± 0.18
66.5 ± 1.2	57.72 ± 10.39	–	–	–	0.94 ± 0.17
68.0 ± 1.2	62.70 ± 11.29	–	–	–	0.96 ± 0.17
68.2 ± 1.2	154.09 ± 27.74	–	–	–	0.275 ± 0.05
71.6 ± 1.1	115.49 ± 20.79	–	–	–	0.63 ± 0.11
75.4 ± 1.1	169.53 ± 30.52	–	–	–	0.89 ± 0.16
76.2 ± 1.1	100.98 ± 18.18	0.08 ± 0.01	–	–	1.35 ± 0.243
77.1 ± 1.0	126.40 ± 22.75	0.09 ± 0.01	–	–	1.17 ± 0.21
78.8 ± 1.0	95.32 ± 17.16	–	–	–	1.2 ± 0.22
81.8 ± 1.0	81.96 ± 14.75	2.48 ± 0.44	–	–	2.35 ± 0.42
82.0 ± 0.9	120.91 ± 21.76	–	–	–	1.37 ± 0.25
85.5 ± 0.6	84.79 ± 15.26	2.21 ± 0.4	–	0.12 ± 0.03	7.88 ± 1.41
85.9 ± 0.9	140.79 ± 28.26	3.11 ± 0.5	–	0.11 ± 0.02	5.15 ± 0.9
88.2 ± 0.6	15.53 ± 2.80	1.53 ± 0.26	0.22 ± 0.05	0.36 ± 0.09	1.03 ± 0.18
88.5 ± 0.8	–	0.42 ± 0.05	0.2 ± 0.05	–	1.58 ± 0.28
91.4 ± 0.6	5.43 ± 0.98	–	0.08 ± 0.02	0.22 ± 0.05	1.15 ± 0.20
93.4 ± 0.8	8.26 ± 1.48	0.4 ± 0.08	0.11 ± 0.02	0.12 ± 0.05	1.5 ± 0.27
94.4 ± 0.6	4.74 ± 0.85	0.2 ± 0.06	0.1 ± 0.03	0.1 ± 0.03	1.33 ± 0.24

the intensities of the characteristic γ rays were used to compute the reaction cross sections at different angular ranges, using Eq. (1), given in Sec. II A of this paper. The efficiency of the detector was obtained for a point source. However, the annular catchers used for trapping the reaction residues had a finite area; therefore, a proper correction [23] was applied to deduce the cross sections for the residues of interest.

III. ANALYSIS

To obtain information regarding the mechanism involved in these reactions, the comparison of measured excitation functions was performed using three computer codes: CASCADE [16], PACE2 [15], and ALICE-91 [17]. Brief details of these codes along with their important parameters, etc., are discussed in the following sections.

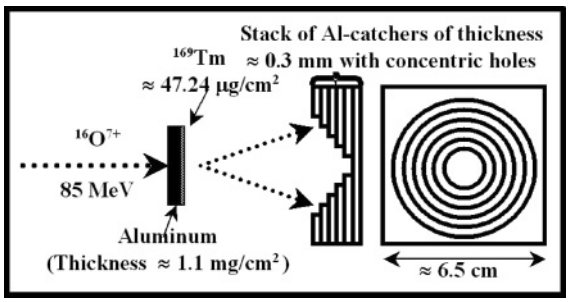

FIG. 4. Typical arrangement of target-catcher assembly used for the angular distribution measurements covering the annular range from 0–13° to 45–60°.

A. Calculations with CASCADE

The code CASCADE [16] is based on Hauser-Feshbach theory [24] and is generally used to obtain the theoretical estimates of cross sections using the CN mechanism. It does not consider the possibility of incomplete fusion (ICF) and PE emission. The main advantage of this code is that it provides the option of scaling the default parameters (i.e., fission barrier, rigid-body momentum of inertia) to obtain cross section values in the mass region of interest. The decay probabilities are

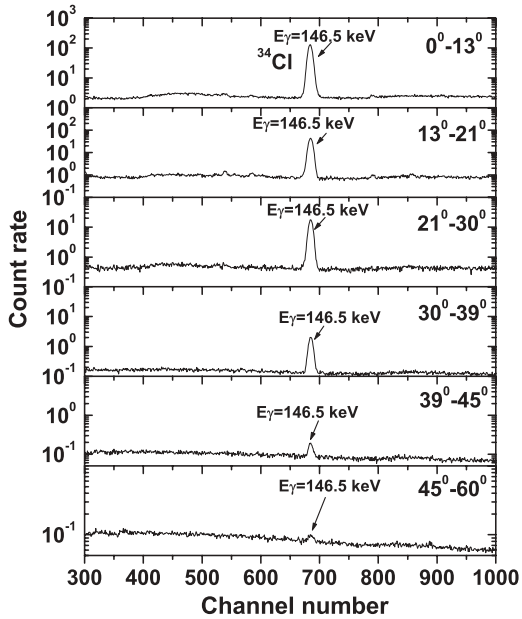

FIG. 5. Typical γ-spectra Al-catcher rings covering the annular range from 0°–13° to 45°–60°.

determined by the level densities of the daughter nuclei and the barrier penetrabilities for the various channels. The optical model potentials of Becchetti and Greenlees [25] are used for calculating the transmission coefficients for protons and neutrons, and the optical model potential of Satchler [26] is used for α particles. The Fermi gas model is used for calculating the level densities for the product nuclei.

The partial cross section for the formation of the compound nucleus of spin J and parity π from a projectile and a target nucleus of spins J_P and J_T, respectively, at center-of-mass energy E is given by [27]

$$\sigma(J,\pi) = \frac{\pi\lambda^2}{4\pi^2}\frac{(2J+1)}{(2J_P+1)(2J_T+1)}\sum_{S=|J_P-J_T|}^{J_P+J_T}\sum_{L=|J-S|}^{J+S} T_L(E), \tag{2}$$

where T_L are the transmission coefficients, which depend on the energy and the orbital angular momentum L, and $S\,(=J_P+J_T)$ is the channel spin.

The total fusion cross section for the maximum angular momentum L_c of the compound nucleus is given by

$$\sigma_L = \frac{\pi\lambda^2}{4\pi^2}\sum_{L=0}^{L_c}(2L+1)T_L(E). \tag{3}$$

In statistical model calculations, the critical angular momentum L_c for compound nucleus fusion may be sharp, or it may have some overlap from L_c to higher L. The effective moment of inertia I may be obtained from the low-lying states of the isotope using the relation

$$I = \frac{2}{5}mr^2, \tag{4}$$

where r is the radius of spherical nucleus given by $r_o A^{1/3}$.

The level density formula implies a yrast line,

$$E_{\rm rot}(J) = \frac{J(J+1)\hbar^2}{2I} + \Delta, \tag{5}$$

where Δ is the pairing energy which determines the zero point of the effective excitation energy. In this code, the level density parameter constant K and the ratio of actual moment of inertia to the rigid-body moment of inertia of the excited system F_θ are the two important parameters which may be varied to match the experimental data. In HI induced reactions, the high angular momentum and excitation energy are expected to have considerable influence on the deexcitation cascade. Because in HI reactions, the increasing excitation energy also increases the angular momentum; therefore, the deformation of the nucleus due to the angular momentum effect may also be quite substantial. In calculations, the deformation effects may be included by using an angular momentum dependent moment of inertia, which results in the deviation of the yrast line from that calculated assuming the nucleus to be a rigid sphere. The level density parameter a_f at the saddle point, which may be obtained from the relation $a_f = A/D_{AF}$, where A is the mass number of the compound nucleus and D_{AF} is a free parameter, may be varied to match the experimental data. It has been observed that the parameter D_{AF} has considerable influence on calculated EFs in the higher energy region.

It may, however, be pointed out that a value of $K > 10$ may give rise to the anomalous effects in particle multiplicity [28]. In the present work, the calculations were performed consistently using the set of parameters which are widely accepted and were used in our recent publication [19]. Here, calculations have been performed taking a value of $K = 8$.

It may also be pointed out that the residue ^{34}Cl produced via the ^{27}Al(^{16}O, $2\alpha n$) channel has metastable as well as ground states. In the present work, the metastable state of the residue ^{34m}Cl was observed through the 146.3 keV γ ray of intensity 40.5%. Since the intensity of the ground state of the residue ^{34g}Cl is very low, the ground state of ^{34g}Cl could not be observed. The production cross sections of the residue ^{34m}Cl were converted into the total cross section of the residue ^{34}Cl by using the standard radioactive decay method. Since the code CASCADE gives the total production cross section of the residue, it is reasonable from a physics point of view to compare the total cross section of the residue ^{34}Cl with the calculations.

The experimentally measured and theoretically calculated EF for the reaction ^{27}Al(^{16}O, $2\alpha n$)^{34}Cl is shown in Fig. 6. The measured values of the cross sections for the residue ^{34}Cl by Landenbaurer-Bellis *et al.* [13], which has some contribution from the residue ^{38}Cl, are also shown. As can be seen from this figure, the measured values [13] of the cross sections of the residue ^{34}Cl have large uncertainties in the energy scale. In the present work, the energy uncertainty resulting from the finite thickness of the sample is much smaller. Furthermore, in the energy range of interest, Landenbaurer-Bellis *et al.* [13] have effectively three data points, whereas in the present work, the measurements were carried out giving 19 data points, indicating a precise measurement at a very close energy interval, as indicated in Fig. 6. As has already been mentioned, the code CASCADE does not take into account the possibility of incomplete fusion processes; therefore, the enhancement of measured cross sections as compared with the calculated EFs for the reaction ^{27}Al(^{16}O, $2\alpha n$)^{34}Cl may be attributed to the ICF process.

The experimentally measured EFs for the reactions ^{27}Al(^{16}O, $3\alpha 3p$)^{28}Mg, ^{27}Al(^{16}O, $3\alpha 3pn$)^{27}Mg, ^{27}Al(^{16}O, $4\alpha 2pn$)^{24}Na, and ^{27}Al(^{16}O, $4\alpha 3p$)^{24}Ne are shown in Figs. 7–10, where the solid curves guide the eye to

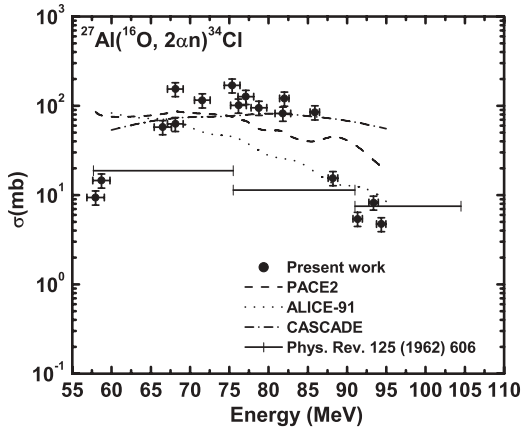

FIG. 6. Experimentally measured and theoretically calculated EFs. Literature values [13] are also shown.

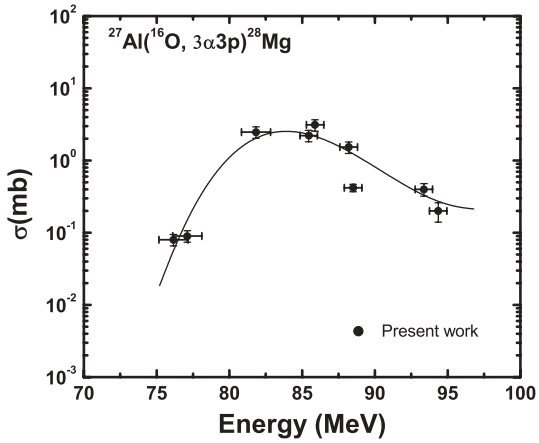

FIG. 7. Experimentally measured EFs. Solid curve guides the eye to the experimental data by curve fitting.

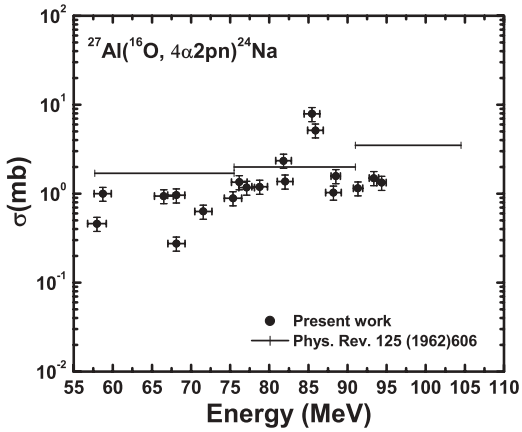

FIG. 9. Experimentally measured EFs. Literature values are also shown.

the experimental data by curve fitting. In Fig. 9, the literature values [13] of the cross sections of the residue ^{24}Na are also shown. On the basis of the trends of these curves, Landenbaurer-Bellis *et al.* [13] concluded that these reactions are formed by evaporation processes referred to as the compound nucleus mechanism. Landenbaurer-Bellis *et al.* [13] in their study of the $^{16}O+^{27}Al$ system did not compare the data with theoretical simulations. Since the calculated values of EFs using code CASCADE for these reactions are negligibly small, they are not shown in Figs. 7–10, thus the observed enhancement by several orders of magnitude over their negligible theoretical predictions for these channels may be attributed to the fact that these reactions are likely to be populated by some processes other than CN processes. Furthermore, to confirm whether these reactions are formed by CF or ICF processes, the angular distributions of these recoiling residues produced in the $^{16}O+^{27}Al$ system have also been measured, as discussed in Sec. IV of the paper.

B. Calculations with PACE2

The theoretical estimate of the cross sections for the evaporation residues has also been obtained using code PACE2 [15], which is based on a statistical approach. It uses a Monte Carlo procedure to determine the decay sequence of an excited nucleus using the Hauser-Fechbach formalism. The angular momentum projections are calculated at each stage of deexcitation, which enables the determination of the angular distribution of the emitted particles. The main advantage of Monte Carlo calculations is that they provide correlations between various quantities, such as particles and γ rays or angular distribution of particles. The evaporation cross sections of the residues are calculated using the Bass formula [29]. The code provides the ability to have an event-by-event traceback of the entire decay sequence from the CN system into any one of the exit channels. The optical model parameters for neutron, proton, and α emission were taken from Perey and Perey [15]. The γ-ray strength functions for $E1$, $E2$, and $M1$ transitions were taken from tables of Endt [30]. This code has been modified to take into account the excitation energy dependence of the level density parameter using the prescription of Kataria *et al.* [31]. In this code, the level density parameter $a = A/K$ is one of the important parameters, where

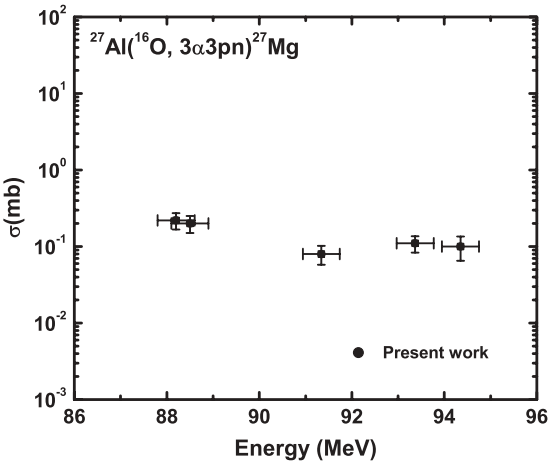

FIG. 8. Experimentally measured EFs.

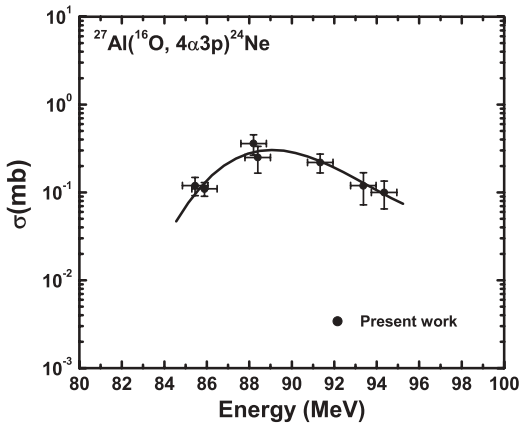

FIG. 10. Experimentally measured EFs. Solid curve guides the eye to the experimental data by curve fitting.

A is the mass number of the compound nucleus and K is a free parameter. The value of K may be varied to match the experimental data. In the present work, a value of $K = 8$ has been taken.

The theoretically calculated EFs using the code PACE2 for the reaction ^{27}Al(^{16}O, $2\alpha n$)^{34}Cl are also shown in Fig. 6 as the dashed curve. The observed enhancement of the measured EFs as compared with the theoretical calculations again indicates that the residue ^{34}Cl may not be produced only by the complete fusion process, but also by some other process such as incomplete fusion. The theoretical calculations for the reactions ^{27}Al(^{16}O, $3\alpha 3p$)^{28}Mg, ^{27}Al(^{16}O, $3\alpha 3pn$)^{27}Mg, ^{27}Al(^{16}O, $4\alpha 2pn$)^{24}Na, and ^{27}Al(^{16}O, $4\alpha 3p$)^{24}Ne give cross sections which are negligibly small, and hence no comparison of the experimental data with the simulations of this code is made in Figs. 7–10. Thus, it may be concluded that the significant contribution to these reaction channels comes from processes other than complete fusion.

C. Calculations with ALICE-91

The code ALICE-91 [17], developed by M. Blann, may be used to calculate the equilibrium as well as preequilibrium (PE) emission cross sections in light and heavy ion induced reactions. The compound nucleus calculations in this code are performed using the Weisskopf-Ewing model [32], while the PE component is simulated using the geometry-dependent hybrid model [33]. In this code, the possibility of incomplete fusion is not taken into account. The particles that could be emitted are neutron, proton, deuteron, and α particles. The code can calculate the reaction cross sections for the residual nuclei up to mass 11 and 9 a.u. away from the compound nucleus. The Myers-Swiatecki/Lysekil mass formula [34] is used for calculating Q values and binding energies of all the nuclei in the evaporation chain. The inverse reaction cross sections used in the code are calculated using the optical model [35] subroutines, although there is also an option of using the classical sharp cutoff model. The transmission coefficients are calculated using the parabolic model of Thomas [36] for heavy ions. Calculations for PE emission in this code are done assuming equipartition of energy among the initial excited particles and holes. The mean free path (MFP) for intranuclear transition rates may be calculated either from the optical model potential parameters of Becchetti and Greenlees [25] or from Pauli-corrected nucleon-nucleon cross sections [37,38]. In the present calculations, the optical potentials of Becchetti and Greenlees [25] were used.

Level densities of the residue in code ALICE-91 may be calculated either from the Fermi gas model or from the constant temperature form. The Fermi gas model gives [39]

$$\rho(U) = (U - \delta)^{-5/4} \exp\left[2\sqrt{a(U - \delta)}\right] \tag{6}$$

where δ is the pairing term and U is the excitation energy of the nucleus. The level density parameter a is taken as A/K, A being the mass number of the nucleus and K is an adjustable parameter. The level density $\rho(U)$ in constant temperature form is given as [40]

$$\rho(U) \propto \frac{1}{T}\varepsilon^{U/T}. \tag{7}$$

The differential cross section for emitting a particle with channel energy ε may be written as (cross section per unit energy to emit a particle of type ν)

$$\frac{d\sigma}{d\varepsilon_\nu} = \frac{\pi\lambda^2}{4\pi^2}\sum_{I=|0|}^{\infty}(2I+1)T_I(2S_\nu+1) \times \sum_{l=|0|}^{\infty}T^l{}_\nu(\varepsilon)\sum_{J=|I-l|}^{I+l}\rho(\varepsilon, J)/D, \tag{8}$$

where λ is the de Broglie wavelength of the incident ion, T_I the transmission coefficient of the Ith partial wave of the incident ion, $\rho(\varepsilon, J)$ the spin-dependent level density for the residual nucleus, D the integral of numerator over all particles and emission energies, and ε the excitation energy of the compound nucleus. S_ν is the intrinsic spin of the particle ν, and $T^l_\nu(\varepsilon)$ is the transmission coefficient for the particle ν with kinetic energy ε and orbital angular momentum l.

In the Weisskopf-Ewing calculations, the nuclear moment of inertia is infinite; hence there is no energy tied to rotation, thus no level density cutoff at high spin. This code does not take into account the angular momentum involved in heavy ion reactions. However, the heavy ion projectile imparts large angular momentum to the composite system having a finite moment of inertia and hence greater rotational energy. Due to nuclear rotation, a nucleus with a given angular momentum J cannot have energy below a minimum value $E_J^{\min}$, that is,

$$E_J^{\min} \approx J(J+1)\frac{\hbar^2}{2I}. \tag{9}$$

Here, I is the moment of inertia of the composite nucleus.

In this code, the level density parameter a, the MFP multiplier COST, and initial exciton number n_0 are some of the important parameters. a largely affects the equilibrium component, while n_0 and COST govern the preequilibrium component. a is calculated from $a = A/K$. In code ALICE-91, the intermediate states of the system are characterized by the excitation energy E and number n_p of excited particles and n_h of excited holes. Particles and holes are defined relative to the ground state of the nucleus and are called excitons. The initial configuration of the compound system defined by the exciton number $n_0 = (n_\mathrm{p} + n_\mathrm{h})$ is an important parameter of PE formalism. In the present work, a value of $n_0 = 16$ with configuration $(8p + 8n + 0\mathrm{h})$ has been found to satisfactorily reproduce the experimental data, where p, n and h represent the number of excited protons, neutrons, and holes, respectively. The code ALICE-91 calculates two-body nuclear transition rates using Pauli-corrected free nucleon-nucleon scattering cross section data. The actual MFP inside the nucleus may be quite different from the one calculated using free nucleon-nucleon scattering data. To compensate for this difference, a parameter COST is provided in the code ALICE-91. A value of COST greater than zero means a smaller value of the actual MFP for nucleon-nucleon scattering inside the composite excited nucleus. In the present work, a value

of COST = 2 is found to reproduce the experimental data satisfactorily.

When ALICE-91 calculations with the above-mentioned parameter values were compared with their experimental counterparts, it was observed that the maxima of the measured EFs were at higher energies than those of the calculated EFs. This is to be expected, because in ALICE-91 calculations the angular momentum effects are not taken into account. In HI induced reactions, the incident particle imparts relatively larger angular momentum to the composite system. If, in the last stages of nuclear deexcitation, higher angular momentum inhibits particle emission more than it does γ emission, then the peak of the excitation function corresponding to the particle emission mode will be shifted to higher energies [41]. The effect is more pronounced in heavy ion reactions than in light ion reactions, since the rotational energy is much greater in HI reactions. An estimate of the possible shift due to angular momentum effects may be made from the nuclear rotational energy. For a rigid body, the rotational energy is given by $E_{\rm rot} \approx (m/M)E_{\rm lab}$. Here, m/M is the ratio of the projectile and target nucleus masses and $E_{\rm lab}$ is the incident energy [41]. Since the angular momentum effects have not been considered in the Weisskopf-Ewing calculations of the present version of the ALICE-91 code, it is desirable to shift the calculated EFs by the amount approximately equal to $E_{\rm rot}$ as calculated above. In the present work, the calculated EFs have been shifted by $E_{\rm rot}$ on the energy scale. The experimentally measured and theoretically calculated EFs for the reaction $^{27}Al(^{16}O, 2\alpha n)^{34}Cl$ are shown in Fig. 6, where the dotted curve shows the theoretical calculation done using code ALICE-91. The observed enhancement of the measured EFs compared with the theoretical calculations for the reaction $^{27}Al(^{16}O, 2\alpha n)^{34}Cl$ done by this code indicates that the residue ^{34}Cl may not be produced by complete fusion but by some other processes such as ICF. Furthermore, the measured EFs for the reactions $^{27}Al(^{16}O, 3\alpha 3p)^{28}Mg$, $^{27}Al(^{16}O, 3\alpha 3pn)^{27}Mg$, $^{27}Al(^{16}O, 4\alpha 2pn)^{24}Na$, and $^{27}Al(^{16}O, 4\alpha 3p)^{24}Ne$ are shown in Figs. 7–10. The theoretical calculations for these reactions give cross sections that are negligibly small, similar to the codes CASCADE and PACE2, while the measured EFs for these channels have substantial cross sections. As such, it may be concluded that after including PE emission, which is one of the dominant mode of reaction mechanisms in heavy ion reactions, the experimental data could not be reproduced, indicating the presence of a reaction mechanism other than CF and PE processes.

IV. ANGULAR DISTRIBUTIONS

The analysis of EFs for the presently measured reactions, as mentioned in Secs. III A–III C, clearly indicates that these reactions have significant contributions other than those of CF and ICF processes. To confirm the reaction mechanism involved, a specially designed experimental setup was used as shown in Fig. 4. In this experiment, an Al target supported by a natural thulium material of thickness $\approx$0.48 mg/cm^2 followed by a stack of thick annular concentric Al catcher foils was used. Depending on the momentum transfer from the projectile to the composite system, the residues formed by CF and ICF processes will be trapped in the concentric annular aluminum catchers at different angles. The residues that are expected to be populated by a mechanism such as a direct reaction may be stopped within the thulium layer. The measured angular distributions for the reaction $^{27}Al(^{16}O, 2\alpha n)^{34}Cl$ is shown in Fig. 11. Two peaks are observed: one around 0°–13° can be assigned to the residues populated by complete fusion, and the other peak in the angular range 45°–60° can be assigned to the residues populated by ICF processes.

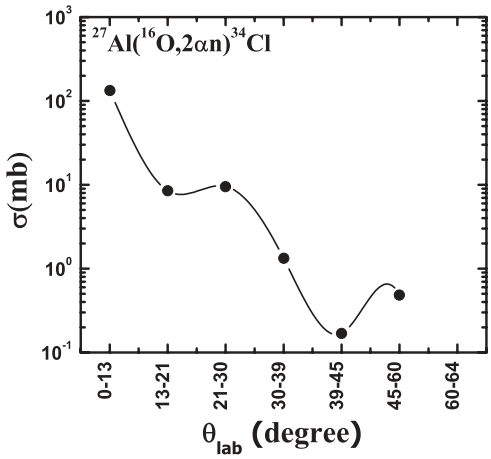

FIG. 11. Measured angular distributions for reaction $^{27}Al(^{16}O, 2\alpha n)^{34}Cl$.

Note that out of the five reactions identified in the EF measurements, only the γ ray of 146.5 keV corresponding to the reaction $^{27}Al(^{16}O, 2\alpha n)^{34}Cl$ could be identified from its energy as well as the half-life of residue ^{34}Cl in the angular distribution measurements. The residues formed by CF are likely to recoil in the forward cone, as such peaking of angular distribution around 0° indicates the population of residue ^{34}Cl via CF. However, the same residue ^{34}Cl when populated by ICF of residue ^{16}O will show peaks at much higher angles. Therefore, it may be concluded that the basic mechanism of population of ^{34}Cl may be based on both CF and ICF processes. However, the EF analysis has clearly indicated that the other reactions, i.e., $^{27}Al(^{16}O, 3\alpha 3p)^{28}Mg$, $^{27}Al(^{16}O, 3\alpha 3pn)^{27}Mg$, $^{27}Al(^{16}O, 4\alpha 2pn)^{24}Na$, and $^{27}Al(^{16}O, 4\alpha 3p)^{24}Ne$, are not likely to be populated via the CF process. The same is reflected from the angular distribution measurements, since no peak corresponding to these residues is identified in the γ-ray spectra of the angular distribution data. Thus, those residues are not likely to be populated via either complete or incomplete fusion processes. In direct reactions, the ejectile takes away a large fraction of the energy; hence, the residues formed may have ranges much smaller than those of residues formed by CF and/or ICF processes and may be trapped in the thulium layer.

V. CONCLUSIONS

Excitation functions for the reactions $^{27}Al(^{16}O, 2\alpha n)^{34}Cl$, $^{27}Al(^{16}O, 3\alpha 3p)^{28}Mg$, $^{27}Al(^{16}O, 3\alpha 3pn)^{27}Mg$, $^{27}Al(^{16}O, 4\alpha 2pn)^{24}Na$, and $^{27}Al(^{16}O, 4\alpha 3p)^{24}Ne$ produced in the $^{16}O+^{27}Al$ system have been measured in the energy range

≈58–94 MeV. Theoretical calculations based on three different computer codes have been carried out using well-accepted parameters. The codes PACE2 and CASCADE used in the present work are based on Hauser-Feshbach theory for compound nucleus calculations; however, the code ALICE-91 is based on the Weisskopf-Ewing model for compound nucleus calculations and the geometry-dependent hybrid model for simulating preequilibrium emission. Though preequilibrium emission may have considerable influence on the measured cross sections at relatively higher energies, even the ALICE-91 calculations which include preequilibrium emission are not found to reproduce the experimental data. The present analysis indicates that the residues ^{27,28}Mg, ^{24}Na, and ^{24}Ne are not populated either via complete or incomplete fusion processes, because theoretical calculations based on all these codes give negligible value of cross sections for their production. At present, we have no satisfactory explanation for the observed high cross sections for these channels; however, Landenbaurer-Bellis *et al*. [13] have attributed their production to a direct reaction mechanism. From the study of the angular distributions of these residues, we have concluded that in the case of complete fusion, the residues are emitted in the forward cone along the beam direction; while for incomplete fusion, the recoiling residues emerge at relatively large angles with respect to the beam direction, as expected. As such, angular distributions of residues with respect to the beam direction may also provide complementary information about the complete and incomplete fusion processes. The analysis of angular distribution data has clearly indicated the significant contribution of the ICF process in the ^{27}Al(^{16}O, $2\alpha n$)^{34}Cl reaction.

ACKNOWLEDGMENTS

The authors are thankful to the Director, NSC, New Delhi, for extending all the facilities for carrying out the experiment. We are also thankful to Dr. R. K. Bhaumik, for all his support during the experiment. We also thank the Chairman, Department of Physics, AMU for providing all the necessary facilities. One of the authors (MKS) thanks the Department of Science and Technology, New Delhi, for providing financial support through Project No. SR/FTP/PS-46/2003.

[1] M. Blann, Nucl. Phys. **A235**, 211 (1974).
[2] M. Blann, Annu. Rev. Nucl. Sci. **25**, 123 (1975).
[3] P. E. Hodgson, *Nuclear Heavy Ion Reactions* (Clarendon, Oxford, 1978).
[4] P. Vergani, E. Gadioli, E. Vaciago, E. Fabrici, E. Gadioli Erba, M Galmarini, G. Ciavola, and C. Marchetta, Phys. Rev. C **48**, 1815 (1993).
[5] M. Crippa, E. Gadioli, P. Vergani, G. Ciavola, C. Marchetta, and M. Bonardi, Z. Phys. A **350**, 121 (1994).
[6] M. Cavinato, E. Fabrici, E. Gadioli, E. Gadioli Erba, P. Vergani, M. Crippa, G. Colombo, I. Redaelli, and M. Ripamonti, Phys. Rev. C **52**, 2577 (1995).
[7] I. Tserruya *et al*., Phys. Rev. Lett. **60**, 14 (1988).
[8] D. J. Parker, J. Asher, T. W. Conlon, and N. Naqib, Phys. Rev. C **30**, 143 (1984).
[9] D. J. Parker, J. J. Hogan, and J. Asher, Phys. Rev. C **35**, 161 (1987).
[10] Manoj Kumar Sharma, Ph.D. thesis, Aligarh Muslim University, 2002.
[11] J. Wilczynaski, K. Siwek-Wilczynaski, J. VanDriel, S. Gonggrip, D. C. J. M. Hangeman, R. V. F. Janssens, J. Lukasiak, R. H. Siemssen, and S. Y. Van der Werf, Nucl. Phys. **A373**, 109 (1982).
[12] S. Chakrborty, B. S. Tomar, A. Goswami, S. K. G. K. Gubbi, S. B. Manohar, Anil Sharma, B. B. Kumar, and S. Mukherjee, Nucl. Phys. **A678**, 355 (2000).
[13] Inge-Maria Ladenbaurer-Bellis, Ivor L. Preiss, and C. E. Anderson, Phys. Rev. **125**, 606 (1962).
[14] P. McKenna *et al*., Phys. Rev. Lett. **91**, 075006 (2003).
[15] A. Gavron, Phys. Rev. C **21**, 230 (1980).
[16] F. Puhlhofer, Nucl. Phys. **A280**, 267 (1977).
[17] M. Blann, NEA Data Bank, Gif-sur-Yvette, France, Report PSR-146, 1991 (unpublished).
[18] M. K. Sharma, Unnati, B. K. Sharma, B. P. Singh, H. D. Bhardwaj, R. Kumar, K. S. Golda, and R. Prasad, Phys. Rev. C **70**, 044606 (2004).
[19] M. K. Sharma, Unnati, B. P. Singh, H. D. Bhardwaj, R. Kumar, K. S. Golda, and R. Prasad, Nucl. Phys. **A776**, 83 (2006).
[20] FREEDOM, Data acquisition and analysis system designed to support the accelerator-based experiments at the Nuclear Science Centre, New Delhi, India.
[21] E. Browne and R. B. Firestone, *Table of Radioactive Isotopes* (John Wiley & Sons, New York, 1986).
[22] M. K. Sharma, B. P. Singh, S. Gupta, M. M. Muthafa, H. D. Bhardwaj, and R. Prasad, J. Phys. Soc. Jpn. **72**, 1917 (2003).
[23] R. P. Gardner and K. Verghese, Nucl. Instrum. Methods **93**, 163 (1971).
[24] W. Hauser and H. Feshbach, Phys. Rev. **87**, 336 (1952).
[25] F. D. Becchetti and G. W. Greenlees, Phys. Rev. **182**, 1190 (1969).
[26] G. R. Satchler, Nucl. Phys. **70**, 177 (1965).
[27] J. M. Blatt and V. F. Weisskopf, *Theoretical Nuclear Physics* (John Wiley & Sons, New York, 1952).
[28] J. P. Lestone, Phys. Rev. C **53**, 2014 (1996).
[29] R. Bass, Nucl. Phys. **A231**, 45 (1974).
[30] P. M. Endt, At. Data Nucl. Data Tables **26**, 47 (1981).
[31] S. K. Kataria, V. S. Ramamurthy, and S. K. Kapoor, Phys. Rev. C **18**, 549 (1978).
[32] V. F. Weisskopf and D. H. Ewing, Phys. Rev. **57**, 472 (1940).
[33] M. Blann, Phys. Rev. Lett. **27**, 337 (1971).
[34] W. D. Myers and W. J. Swiatecki, Ark. Fys. **36**, 343 (1967).
[35] M. Blann, Phys. Rev. C **21**, 1770 (1980).
[36] T. D. Thomas, Nucl. Phys. **53**, 577 (1964).
[37] K. Kikuchi and M. Kawai, *Nuclear Matter and Nuclear Reactions* (North-Holland, Amsterdam, 1968).
[38] M. Blann, Nucl. Phys. **A213**, 570 (1973).
[39] M. Blann and H. Vonach, Phys. Rev. C **28**, 1475 (1983).
[40] M. Blann, G. Reffo, and F. Fabbri, Nucl. Instrum. Methods A **265**, 490 (1988).
[41] D. Bodansky, Annu. Rev. Nucl. Sci. **12**, 79 (1962).